

This item was submitted to Loughborough's Institutional Repository (<https://dspace.lboro.ac.uk/>) by the author and is made available under the following Creative Commons Licence conditions.



CC creative commons
COMMONS DEED


Attribution-NonCommercial-NoDerivs 2.5


You are free:

- to copy, distribute, display, and perform the work

Under the following conditions:

 **Attribution.** You must attribute the work in the manner specified by the author or licensor.

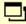
 **Noncommercial.** You may not use this work for commercial purposes.

 **No Derivative Works.** You may not alter, transform, or build upon this work.

- For any reuse or distribution, you must make clear to others the license terms of this work.
- Any of these conditions can be waived if you get permission from the copyright holder.

Your fair use and other rights are in no way affected by the above.

This is a human-readable summary of the [Legal Code \(the full license\)](#).

[Disclaimer](#) 

For the full text of this licence, please go to:
<http://creativecommons.org/licenses/by-nc-nd/2.5/>

Computer simulations of evaporation of sessile liquid droplets

S. Semenov^a, V.M. Starov^{a,*}, R.G. Rubio^b, M.G.Velarde^c

^a Dept. of Chemical Engineering, Loughborough University, LE11 3TU Loughborough, UK,
e-mails: S.Semenov@lboro.ac.uk, V.M.Starov@lboro.ac.uk

^b Dept. of Química Física I, Universidad Complutense, 28040 Madrid, Spain,
e-mail: rgrubio@quim.ucm.es

^c Instituto Pluridisciplinar, Universidad Complutense, 28040 Madrid, Spain,
e-mail: mgvelarde@pluri.ucm.es

Abstract

Computer simulations of the evaporation of sessile droplets are carried out in a self consistent way by considering an interconnected problem of vapour transfer, heat transfer in vapour, liquid and solid substrate, and Marangoni convection inside the liquid droplet. The influence of thermal conductivity of the solid support on the evaporation process is evaluated. It is shown that the lower the thermal conductivity of the solid substrate the higher is the deviation from the isothermal case. However, if the mean temperature of the droplet surface is used instead of the temperature of the surrounding air for the vapour concentration on the droplet surface then the calculated dependences coincide with those calculated for the isothermal case.

Keywords: evaporation, sessile droplets, computer simulations.

* To whom correspondence should be addressed: Department of Chemical Engineering, Loughborough University, Ashby Rd, Loughborough, Leicestershire, LE11 3TU, UK, e-mail: V.M.Starov@lboro.ac.uk, Tel: +44(0)1509 222508, Fax: +44(0)1509 223923

1. Introduction

Understanding the evaporation of droplets is essential for processes like painting, coating, ink-jet printing, premixing of fuel with oxygen in air [1], particle deposition applications (formation of ring-like spots on the substrate during droplets evaporation), DNA chip manufacturing [2], etc. The measurements of evaporation rate of droplets on different solid surfaces can be used for production of materials providing optimal regime of work in air conditioners, dryers and cooling systems [3]. On the other hand the investigation of evaporating droplets can reveal the influence of Derjaguin pressure in a vicinity of the apparent three-phase contact line [4] as well as the effect of latent heat of vaporization and Marangoni convection [5] on evaporation process.

Evaporation starts after the deposition of a liquid droplet on a solid substrate in a non-saturated vapour atmosphere. In the presence of contact angle hysteresis the latter process occurs in three steps [6, 7]. During the first step evaporation proceeds with a constant radius of the droplet base, L , and decreasing contact angle, θ , until the contact angle reaches the static receding value, θ_r . The second stage of evaporation develops at constant contact angle, θ_r , and decreasing radius of the droplet base, L . During the third stage both the radius of the droplet base, L , and the contact angle, θ , decrease until the droplet disappears. The first stage is usually the longest one and lasts until the contact angle reaches, θ_r . The third stage is the shortest one and the most difficult for experimental investigation.

R.D. Deegan *et al* [8, 9] studied the distribution of vapour flux density over the spherical cap of a sessile droplet neglecting the latent heat of vaporization and the thermocapillary flow inside the droplet. Their solution for droplets with contact angles $\theta < 90^\circ$ shows an increased vapour flux in the vicinity of the three-phase contact line. Such distribution of the flux over the droplet surface, according to the authors, generates flow inside the droplet, which transports suspended solid particles to the edge of the droplet thus leading to a ring-like stain formation.

A.M. Cazabat *et al* [10] showed that the vapour flux density over the droplet is inversely proportional to the radius of the droplet base. As a consequence the integration of flux density over the whole droplet surface gives a total vapour flux proportional to the radius of the droplet base.

Theoretical and computer simulation studies [5, 11–15] give the following equation for the evaporation rate of a sessile droplet:

$$\frac{dV}{dt} = -2\pi \frac{DM}{\rho} (c(T_{surf}) - Hc(T_\infty)) F(\theta) L, \quad (1)$$

where V is the droplet volume, t is time, D , ρ , and M are vapour diffusivity in air, density of the liquid and the molar mass, respectively; H is humidity of the ambient air, T_{surf} is the temperature of the droplet-air interface and T_∞ is the temperature of the ambient air, $c(T_{surf})$ and $c(T_\infty)$ are the molar concentrations of saturated vapour at the corresponding temperature; $F(\theta)$ is a function of the contact angle, θ , with value 1 at $\theta = \pi/2$. Eq. (1) was obtained for a model of evaporation which takes into account diffusion only of the vapour in the surrounding air and ignores the temperature distribution along the droplet-air interface. In the case of θ independent of L (second stage of evaporation) Eq.

(1) gives an evaporation rate directly proportional to the radius of the droplet base, L .

Investigations of evaporation of droplets with contact angles $\theta < 120^\circ$ were performed by F. Girard *et al* [5, 12–15] and H. Hu and R.G. Larson [16–18]. The former investigated the influence of substrate heating [14–15], air humidity [14] and Marangoni convection [5]. They concluded that the contribution of Marangoni convection to the total vapour flux is negligible, whereas heating the substrate is significant. The other authors investigated the process of particle deposition and ring-like stain formation during droplet evaporation.

In all mentioned publications either only vapour diffusion was taken into account and both the latent heat of vaporization and Marangoni convection were ignored, or a special form of the vapour flux was postulated and, based on that, other phenomena were investigated.

There we investigate the evaporation process in a self consistent way: we study the interconnected problem of vapour transfer, heat transfer in vapour, liquid and solid substrate, and Marangoni convection inside the liquid droplet.

2. Mathematical modelling and approximations

The system under consideration is a pinned sessile droplet of a liquid on a solid substrate open to ambient air. To simplify the problem is taken axisymmetric with a cylindrical system of coordinates r and z (Fig. 1). To further simplify we focus attention on relatively small droplets, that is, $L \ll a$,

where $a = \sqrt{\frac{\gamma}{\rho g}}$ is the capillary

length, γ is the liquid-air interfacial tension, ρ the liquid density and g is the gravitational acceleration. Hence, in our case here, the static Bond number, Bo , is very

small: $Bo = \frac{\rho g L^2}{\gamma} \ll 1$. For

aqueous droplets: $\rho = 10^3 \text{ kg/m}^3$,
 $\gamma = 0.073 \text{ N/m}$, $L = 0.001 \text{ m}$,

$g \approx 10 \text{ m/s}^2$ and $Bo \approx 0.1 \ll 1$.

Thus the droplet is a spherical segment or better a semicircle cross-section with a fixed contact angle, θ .

The local evaporation rate is limited by the diffusion rate to the ambient air in the vicinity of the evaporating surface and by the transfer rate of molecules from the liquid phase to the gaseous phase [13]. The time scale required for a molecule to move from the liquid to the gaseous phase, t_{tr} , can be estimated as l/\bar{v} , where l is the width of the transition zone between the phases, and \bar{v} is the mean square velocity of molecules. If we estimate the width of the transition zone, l , between two phases equal to several mean free molecular paths, then $t_{tr} \sim 10^{-10} \text{ s}$. The time scale required for diffusion, t_{dif} , of a molecule over the distance L is $t_{dif} = L^2/D \sim 10^{-2} \text{ s}$, where D is the molecular

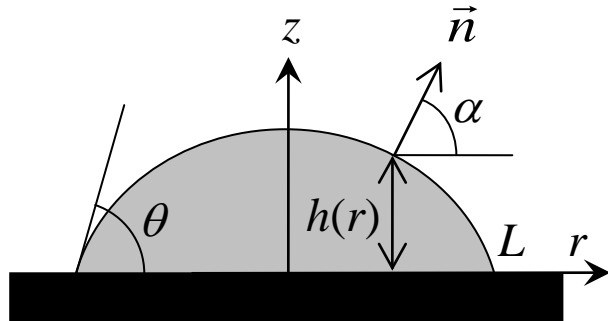


Fig. 1. Evaporating droplets.

diffusion coefficient. As $t_{tr} \ll t_{dif}$ the process of transition of molecules across the interface is much faster than the vapour diffusion. Hence, the evaporation process is governed by diffusion in the ambient air. On the other hand, the time scale of molecular diffusion, t_{dif} , is much smaller than the characteristic time scale of droplet evaporation, t_{evap} , which is usually about 10^2 s [19]. Consequently, the diffusion process can be considered as a quasi-steady process.

The characteristic time scales of heat, t_{heat} , and momentum, t_{mom} , transfer processes inside the droplet are approximately $t_{heat} = L^2 / \kappa \sim 10$ s $\sim 0.1 \cdot t_{evap}$, where κ is the thermal diffusivity of water and $L = 10^{-3}$ m as above, $t_{mom} = \rho L^2 / \eta \sim 1$ s $\sim 0.01 \cdot t_{evap}$, where η is the dynamic (shear) viscosity of water. Those characteristic time scales, t_{heat} and t_{mom} , are smaller than the droplet evaporation time at least by one order of magnitude. For this reason all those processes are taken as steady state processes.

Convection in air is neglected, because the experiments [19] did not reveal any difference in evaporation regimes with and without forced convection in the ambient air. Such assumption is justified below.

2.1. Evolution equations

Let us start considering the particular case of contact angle $\theta = \pi / 2$. In this case we can solve the problem of evaporation of a spherical droplet in three dimensions and a half of the droplet gives a solution for a droplet on a solid substrate with a zero flux through the solid because of symmetry (Fig. 2) and contact angle $\theta = \pi / 2$. In this case the equation, which governs the

evaporation, is: $\frac{1}{r^2} \frac{\partial}{\partial r} \left(r^2 \frac{\partial c}{\partial r} \right) = 0$, with boundary conditions:

$c(L) = c_{sat}(T_{surf})$, $c(\infty) = c_{\infty}$, where $c_{sat}(T_{surf})$ is the concentration of the saturated vapour on the droplet surface and we neglect the deviation of the latter from the actual one (according to the Kelvin's equation [20]). c_{∞} denotes a value in the ambient air far away from the droplet. The solution of the latter

equation with its boundary conditions is $c(r) = c_{\infty} + (c_{sat}(T_{surf}) - c_{\infty}) \frac{L}{r}$. The

local normal vapour flux from the droplet surface is

$$j_{\pi/2}(L, T_{surf}) = D(c_{sat}(T_{surf}) - c_{\infty}) \frac{1}{L}. \quad (2)$$

The latter equation shows that the local flux is constant along the surface and inversely proportional to L . The total flux through the surface of the droplet with contact angle $\theta = \pi / 2$ (half of the droplet in Fig. 2) is

$$J_{\pi/2}(L, T_{surf}) = 2\pi D(c_{sat}(T_{surf}) - c_{\infty}) L, \quad (3)$$

that is proportional to the radius of the droplet (not to the area of its surface) in spite of the invariance of the local normal flux $j_{\pi/2}(L, T_{surf})$ with respect to the position at the surface. This analytical solution, obtained for $\theta = \pi / 2$, is used to validate the computer simulations below.

Let us show that there is inverse proportionality of the local flux to L similar to (2) and the proportionality of the total flux to L similar to (3) remains

valid in the general case of an arbitrary contact angle and has nothing to do with flux distribution over the droplet surface.

Under steady state conditions the distribution of vapour concentration in the ambient air, $c(z, r)$ is described by

$$\frac{1}{r} \frac{\partial}{\partial r} \left(r \frac{\partial c}{\partial r} \right) + \frac{\partial^2 c}{\partial z^2} = 0. \quad (4)$$

The local normal flux, j , on the surface of the droplet

$$j = -D \frac{\partial c}{\partial \vec{n}} \Big|_{z=h(r)} = -D \left[\frac{\partial c}{\partial r} \Big|_{z=h(r)} \cos \alpha + \frac{\partial c}{\partial z} \Big|_{z=h(r)} \sin \alpha \right], \quad (5a)$$

where α is the angle shown in Fig. 1. Let us introduce dimensionless variables using the same symbols as the original dimensional ones but with an overbar: $\bar{z} = z/L$, $\bar{r} = r/L$, $\bar{c} = c/c_\infty$, $\bar{h} = h/L$, then

$$j = -D \frac{\partial c}{\partial \vec{n}} \Big|_{z=h(r)} = -\frac{Dc_\infty}{L} \left(\frac{\partial \bar{c}}{\partial \bar{r}} \Big|_{\bar{z}=\bar{h}(\bar{r})} \cos \alpha + \frac{\partial \bar{c}}{\partial \bar{z}} \Big|_{\bar{z}=\bar{h}(\bar{r})} \sin \alpha \right) = \frac{Dc_\infty}{L} A(\bar{r}, \bar{z}), \quad (5b)$$

where $A(\bar{r}, \bar{z}) = -\left(\frac{\partial \bar{c}}{\partial \bar{r}} \Big|_{\bar{z}=\bar{h}(\bar{r})} \cos \alpha + \frac{\partial \bar{c}}{\partial \bar{z}} \Big|_{\bar{z}=\bar{h}(\bar{r})} \sin \alpha \right)$. The total flux is

$$J = 2\pi \int_0^L r j \sqrt{1 + \left(\frac{\partial h}{\partial r} \right)^2} dr = 2\pi L D c_\infty \int_0^1 \bar{r} A(\bar{r}, \bar{z}) \sqrt{1 + \left(\frac{\partial \bar{h}}{\partial \bar{r}} \right)^2} d\bar{r}. \quad (6)$$

Hence, according to Eqs. (5) and (6), the local flux is $j \sim \frac{1}{L}$ and the total flux is $J \sim L$.

The latter property does not depend on the increase or decrease of the vapour flux in a vicinity of the three-phase contact line.

Now let us estimate the influence of air convection on the evaporation process. The air velocity will have both tangential (caused by no-slip boundary condition at the liquid-air interface) and normal (due to evaporation components at the droplet surface). Consequently, the tangential component depends on the thermal Marangoni convection in the droplet ($\sim 10^{-3}$ m/s according to computer simulations), and the normal component is defined by the local evaporation rate j :

$$u_{n,a} = \frac{j_\rho}{\rho_a} \approx \frac{jM}{\rho_a},$$

where $u_{n,a}$ is the normal air velocity at the droplet surface, j_ρ is the normal local mass flux due to evaporation, ρ_a is the density of air, j is the normal local molar flux of vapour, M is the molar mass of vapour. For the case of contact angle $\theta = \pi/2$, humidity $H = 70\%$, droplet base radius $L = 10^{-3}$ m and surface

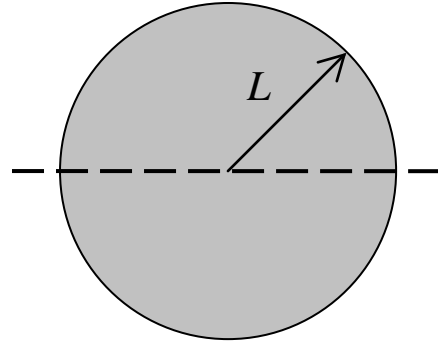


Fig. 2. Evaporating spherical droplet.

temperature $T_{surf} = 293$ K we can estimate the local vapour flux $j_{\pi/2}$ using Eq. (2). The result is $u_{n,a} \sim 10^{-4}$ m/s. Hence, the characteristic convection velocity of air $u_a = 10^{-3}$ m/s. Using that characteristic velocity, characteristic droplet size $L = 10^{-3}$ m, as well as the vapour diffusion coefficient $D = 2.4 \cdot 10^{-5}$ m²/s and the thermal diffusivity of air $\kappa = 2.0 \cdot 10^{-5}$ m²/s, we can calculate the thermal, Pe_κ , and the diffusive, Pe_D , Peclet numbers: $Pe_\kappa = Lu/\kappa = 0.05$; $Pe_D = Lu/D \approx 0.04$. Such low values of Peclet numbers mean that the convective fluxes of heat and mass are negligible in comparison with diffusive ones.

From the above estimations we can conclude that air convection can be neglected. A numerical experiment was conducted to cross-check it by considering evaporation of a sessile droplet with air convection and without it. The result shows that the change of temperature at the droplet apex (minimal temperature in the system) is very small:

$$\frac{T_{apex}^{conv} - T_{apex}}{T_\infty - T_{apex}} < 0.01,$$

where T_{apex}^{conv} and T_{apex} are the temperature of the droplet apex with and without air convection, respectively, T_∞ is the ambient temperature far away from the droplet.

The following equations are solved numerically during the simulation of the steady state process of droplet evaporation:

- 1) Eq. (4) describing vapour diffusion in the ambient air;
- 2) The Navier-Stokes equations together with the continuity equation in the liquid bulk:

$$u \frac{\partial u}{\partial r} + v \frac{\partial u}{\partial z} = -\frac{\partial p}{\partial r} + \eta \left(\frac{1}{r} \frac{\partial}{\partial r} \left(r \frac{\partial u}{\partial r} \right) + \frac{\partial^2 u}{\partial z^2} - \frac{u}{r^2} \right), \quad (7)$$

$$u \frac{\partial v}{\partial r} + v \frac{\partial v}{\partial z} = -\frac{\partial p}{\partial z} + \eta \left(\frac{1}{r} \frac{\partial}{\partial r} \left(r \frac{\partial v}{\partial r} \right) + \frac{\partial^2 v}{\partial z^2} \right),$$

$$\frac{1}{r} \frac{\partial(ru)}{\partial r} + \frac{\partial v}{\partial z} = 0, \quad (8)$$

where u and v are radial and vertical components of the velocity vector, respectively, p is the pressure, and η is the dynamic (shear) viscosity;

- 3) The heat transfer Fourier equation in all three phases (solid support, liquid droplet, and the ambient air):

$$u \frac{\partial T}{\partial r} + v \frac{\partial T}{\partial z} = \kappa \left(\frac{1}{r} \frac{\partial}{\partial r} \left(r \frac{\partial T}{\partial r} \right) + \frac{\partial^2 T}{\partial z^2} \right), \quad (9)$$

where T is the temperature, κ is the thermal diffusivity of the corresponding phase. Note that $u = v = 0$ inside vapour and solid phases.

2.2. Boundary conditions

At the liquid-solid boundary no-penetration and no-slip boundary conditions are used for Navier-Stokes equations:

$$u = 0, \quad v = 0;$$

and continuity conditions for the temperature and heat fluxes:

$$T_l = T_s, \quad (10)$$

$$-k_l(\nabla T)_l \cdot \vec{n}_{l,s} = -k_s(\nabla T)_s \cdot \vec{n}_{l,s}, \quad (11)$$

where subscripts l and s refer to liquid and solid phase, respectively, k is the thermal conductivity, ∇T is the temperature gradient, $\vec{n}_{l,s}$ is the unit normal vector, to the liquid-solid interface.

At the air-solid boundary the no-penetration condition is used for the diffusion equation:

$$\vec{j} \cdot \vec{n}_{a,s} = 0, \quad (12)$$

where the subscript a means air phase, $\vec{n}_{a,s}$ is the unit vector, normal to the air-solid interface; continuity for the temperature and the heat fluxes is assumed:

$$T_a = T_s, \quad (13)$$

$$-k_a(\nabla T)_a \cdot \vec{n}_{a,s} = -k_s(\nabla T)_s \cdot \vec{n}_{a,s}. \quad (14)$$

Symmetry demands:

$$\left. \frac{\partial c}{\partial r} \right|_{r=0} = 0, \quad \left. \frac{\partial T}{\partial r} \right|_{r=0} = 0, \quad \left. \frac{\partial v}{\partial r} \right|_{r=0} = 0, \quad u = 0. \quad (15)$$

At the outer boundaries of the system the following conditions are applied:

$$c(\infty) = c_\infty, \quad T(\infty) = T_\infty. \quad (16)$$

Under steady state conditions the velocity component normal to the liquid-air boundary is zero:

$$\vec{u} \cdot \vec{n}_{l,a} = 0, \quad (17)$$

where $\vec{n}_{l,a}$ is the unit normal vector to the liquid-air interface.

The thermal Marangoni stress condition is used at the liquid-air interface:

$$\boldsymbol{\tau} \cdot \vec{n}_{l,a} = -\gamma K \vec{n}_{l,a} + \gamma'_T \nabla_{surf} T, \quad (18)$$

where $\boldsymbol{\tau}$ is the full stress tensor, γ is the liquid-air interfacial tension, K is the curvature of the liquid-air interface (positive for a droplet), γ'_T is the derivative of γ with temperature, $\nabla_{surf} T = \left(\frac{\partial T}{\partial r} \sin \alpha - \frac{\partial T}{\partial z} \cos \alpha \right) \vec{s}_{a,l}$ is the surface gradient of the temperature, $\vec{s}_{a,l}$ is the unit tangent vector at the liquid-air interface.

The concentration of saturated vapour, c_{sat} , at the droplet surface is defined by the local temperature according to the Clausius-Clapeyron equation and the ideal gas law:

$$\ln \left(\frac{p_{sat}}{p_{sat\infty}} \right) = -\frac{\Lambda}{R} \left(\frac{1}{T} - \frac{1}{T_\infty} \right), \quad (19)$$

$$p_{sat} = c_{sat} RT, \quad (20)$$

where p_{sat} is the pressure of saturated vapour at temperature T , $p_{sat\infty}$ is the pressure of saturated vapour at temperature T_∞ , Λ is the latent heat of vaporization of the liquid and R is the universal gas constant. The value of c_{sat} is noticeably affected by the curvature of the droplet surface according to the Kelvin's equation only at a relatively small size of the droplet: the change constitutes more than 1% if the droplet size is less than 10^{-7} m. The latter is four orders magnitude smaller than that of the droplet sizes under

consideration. Therefore the influence of curvature on the concentration of saturated vapour is neglected below.

The temperature at the liquid-air interface is continuous:

$$T_l = T_a. \quad (21)$$

However the heat flux experiences discontinuity because of the latent heat of vaporization:

$$k_a (\nabla T)_a \cdot \vec{n}_{l,a} - k_l (\nabla T)_l \cdot \vec{n}_{l,a} = j \cdot \Lambda. \quad (22)$$

2.3. Numerical simulations

The solution of the steady state problem described above was performed using the commercial software COMSOL Multiphysics v 3.5a. The numerical technique used by that software is the Finite Element Method (FEM). The shape functions, chosen for the simulation, are Lagrange quadratic shape functions.

The shape of the air domain is chosen to be a hemisphere above the droplet with boundary conditions at its outer boundary Eq. (16). The radius of this hemisphere is chosen to be one hundred times bigger than the droplet base radius L . This choice prevents numerical artefacts caused by the proximity of the outer boundary [14], and provides a good approximation (less than 1% error bar) for the problem of droplet evaporation into a semi-infinite space.

The mesh generated consists of triangular elements, whose size is changing gradually from the smallest value at the droplet edge to the biggest one at the outer boundary of the air domain.

The evaporation flux and viscous stress both diverge to infinity at the droplet edge (for $\theta \neq \pi/2$), which is due to the incompatibility of the boundary conditions at the liquid-air interface and those of the liquid-substrate and gas-substrate interfaces. Therefore, to reduce the influence of singularities on the problem solution the size of mesh elements at the droplet edge is chosen to be one hundred times smaller than the droplet base radius, L . In all our computer simulations the liquid used is water and the solid substrate is made of copper if other materials are not mentioned. $T_\infty=20^\circ\text{C}$ is used below.

3. Results and discussion

Unlike lab experiments computer simulations allow to switch off and on any physical effects in the system under consideration. Initially we switch off both the Marangoni convection and the effect of latent heat of vaporization. It allows comparing our simulation results with earlier published results on evaporation of droplets.

3.1. Local normal vapour flux over the droplet surface

The distribution of local normal vapour flux, j , over the droplet surface is shown in Fig. 3. It is done using a rescaled, normalised vapour flux $j/j_{\pi/2}(L, T_\infty)$, where $j_{\pi/2}(L, T_\infty)$ is the flux when $\theta = \pi/2$ and $T_{surf} = T_\infty$ according to Eq. (2), when only diffusion of the vapour is taken into account. In Fig. 3 three different cases are presented: 1) evaporation with both the Marangoni convection (MC) and latent heat of vaporization (LHV) included; 2) evaporation with LHV included but without MC; 3) evaporation without both MC and LHV. The latter corresponds to the above mentioned analytical

solution, $j_{\pi/2}(L, T_\infty)$, Eq. (2). The line with triangles (Fig. 3), gives the result, which coincides with the analytical solution (the straight line): $j/j_{\pi/2}(L, T_\infty) = 1$ within the simulation error bar.

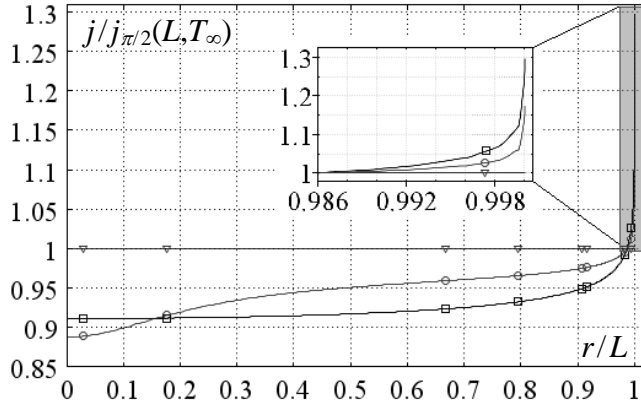


Fig. 3. Calculated distributions of local normal vapour flux, j , over the droplet surface, $\theta = \pi/2$, $L = 1$ mm. Circles - both Marangoni convection (MC) and latent heat of vaporization (LHV) are taken into account; squares - LHV is included, but MC is excluded; triangles - both MC and LHV are excluded. The insertion represents the shaded rectangle with a changed scale.

ambient temperature because of the proximity of highly heat conductive substrate (Fig. 4). A redistribution of the vapour concentration over the droplet surface causes a redistribution of vapour concentration in the ambient air. As a result there is up to 10% decrease of j over the droplet surface (due to temperature decrease), and up to 30% increase of j at the droplet edge (due to constant temperature and vapour concentration redistribution), as illustrated in Fig. 3.

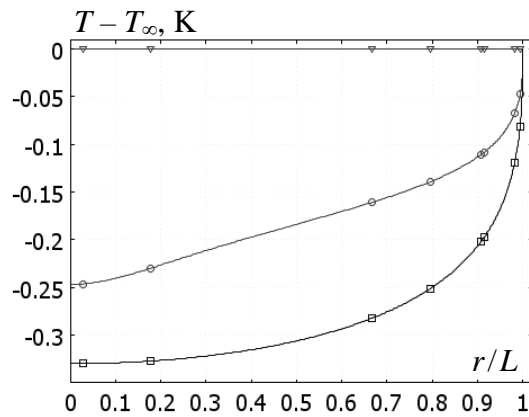


Fig. 4. Calculated temperature distributions over the droplet surface: $\theta = \pi/2$, $L = 1$ mm. T_∞ is the ambient temperature. Circles - MC and LHV are taken into account; squares - LHV is included, but MC is excluded; triangles - both MC and LHV are excluded.

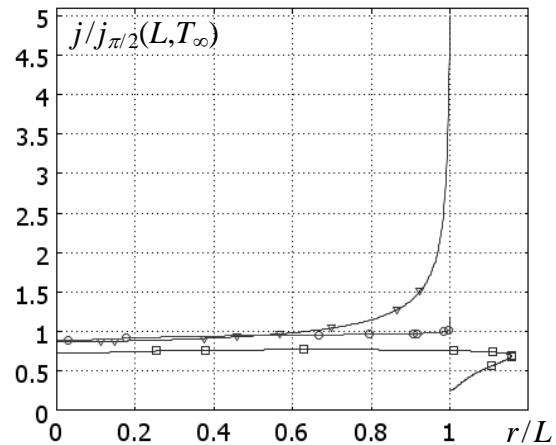


Fig. 5. Calculated distributions of local normal vapour flux, j , over the droplet surface, $L = 1$ mm, both LHV and MC are taken into account. Circles - $\theta = \pi/2$; squares - $\theta = 2\pi/3$; triangles - $\theta = 2\pi/9$.

LHV reduces the local flux of evaporation, j , over the whole surface except at the droplet edge, where it increases (squares in Fig. 3). The latter is caused by a redistribution of vapour concentration over the surface according to the surface temperature. The temperature decrease over the whole droplet is caused by the heat consumption by the evaporation (Fig. 4). However, the lower is temperature the lower is the saturated vapour concentration, $c_{sat}(T_{surf})$. The temperature at the droplet edge remains equal to the

Inclusion of Marangoni convection inside the droplet (Fig. 6) provides a convective heat flux in addition to the conductive flux. The flow along the surface from the edge of the droplet, where the temperature is higher, to the apex increases the temperature at the droplet surface. However, the convective heat flux from the droplet apex down to the substrate decreases the temperature of the apex. Such temperature change (Fig. 4) results in a corresponding vapour concentration change and, as a consequence, the local vapour flux changes (Fig. 3).

The distribution of the local vapour flux, j , is affected by the contact angle θ (Fig. 5). When $\theta < \pi/2$, the local flux increases towards the three-phase contact line. However, if $\theta > \pi/2$, the situation is the opposite. These results are in a qualitative agreement with the result of Deegan *et al* [9], who calculated the vapour flux taking into account the vapour diffusion only in an isothermal case.

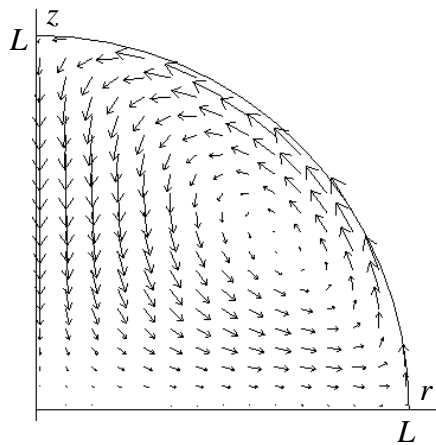


Fig. 6. Velocity field inside the droplet with $\theta = \pi/2$ and $L = 1$ mm. Both LHV and MC are taken into account.

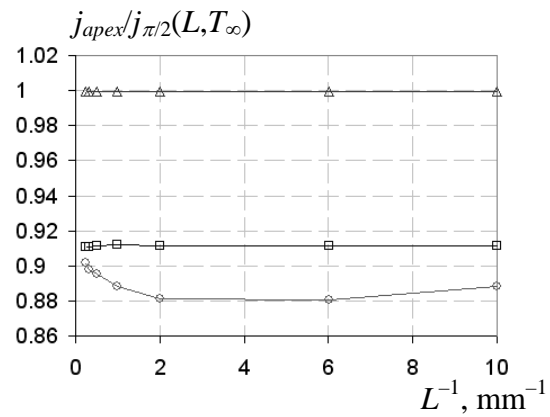


Fig. 7. Calculated dependences of a local vapour flux at the droplet apex, j_{apex} , on radius of the droplet base, L ; $\theta = \pi/2$. Circles - MC and LHV are taken into account; squares - LHV is included, but MC is excluded; triangles - both MC and LHV are excluded.

To check the validity of the above given relationship for the local vapour flux, $j \sim 1/L$, Eq. (5), the ratio of fluxes $j_{apex}/j_{\pi/2}(L, T_{\infty})$ was plotted against the inverse value of L (Fig. 7) for the case $\theta = \pi/2$. Equation (5) is valid according to Fig. 7 only when the Marangoni convection is neglected: the presence of the Marangoni convection makes non-linear this dependence (circles in Fig. 7).

3.2. Total vapour flux from the droplet surface

Let us now study the dependence of the total vapour flux, J , on the radius of the droplet base, L , and the contact angle, θ (Fig. 8). It appears that J increases nonlinearly with contact angle. All calculations were performed with both LHV and MC included. The results (Fig. 8) were obtained for substrates made of different materials and compared to those calculated for the isothermal case by H. Hu and R.G. Larson [16] and F. Schonfeld *et al* [21]. In the case of highly heat conductive solid support (copper) the difference between the present simulations and the results from [16, 21] for isothermal case do not exceed 3%. The latter is because of a small

temperature change at the droplet surface, which is close to isothermal conditions (Fig. 4). However, if other materials are used with lower heat conductivity (down to the heat conductivity of air), then the evaporation flux is substantially reduced (Fig. 8). Such flux reduction is connected to the noticeable temperature reduction of the droplet surface.

Let us now introduce the mean temperature of the droplet surface:

$$T_{av} = \frac{1}{S} \int_S T dS, \text{ where } S \text{ is the droplet surface area. We have plotted the}$$

dimensionless total flux $J/J_{\pi/2}(L, T_{av})$, (Fig. 9). All calculated total fluxes for all substrates are on one universal dependence of total vapour flux, J , versus contact angle, θ . Accordingly, the variation of the surface temperature is the major phenomenon influencing the evaporation rate.

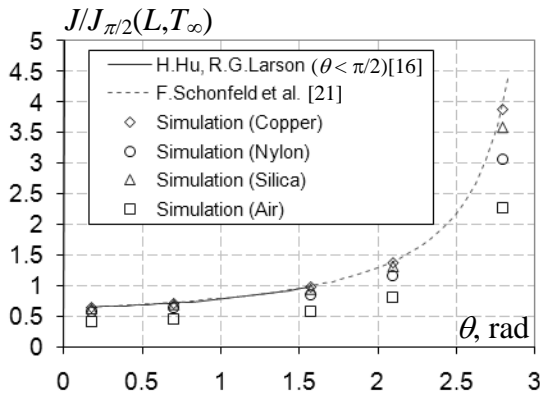


Fig. 8. Rescaled dependence of the total vapour flux from the droplet surface, J , on contact angle θ , $L = 1$ mm. Both LHV and MC are taken into account.

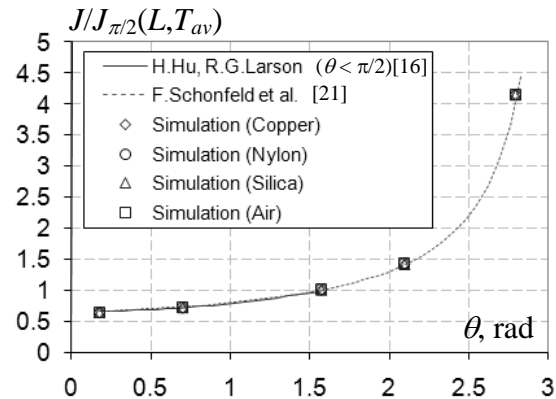


Fig. 9. Rescaled dependence of the total vapour flux from the droplet surface, J , on contact angle θ , $L = 1$ mm. Both LHV and MC are taken into account.

Let us check if the singularity at the droplet edge affects the dependence, presented in Fig. 9. The following procedure was adopted: the singularity region (close to the three-phase contact line) was excluded from the integration of the local vapour flux, j . That is the integration was performed over the part of the surface corresponding to the following range of radial coordinate values: $0 \leq r < 0.95L$; after that the total vapour fluxes J and $J_{\pi/2}(L, T_{av})$ were calculated by integration over a truncated area of the droplet. As a result a deviation from the dependence, presented in Fig. 9 was found to be not more than 2%. That means that the influence of the singularity in the present simulations is negligible.

The total vapour flux, J , varies linearly with L only in the case of absence of Marangoni convection. That can be seen from Fig. 10, where the triangles show the ratio $J(L)/J_{\pi/2}(L, T_{\infty})$ to be constant for the isothermal model while the squares illustrate the constancy for the model with LHV and without MC. The difference between these two is only quantitative: the total evaporation rate is smaller, if LHV is included into the model.

The addition of Marangoni convection changes the character of the above dependence. It becomes non-linear (circles in Fig. 10). For any value of L the evaporation is enhanced if Marangoni convection is included. This evaporation enhancement is due to surface temperature increase (Fig. 4).

As the size of the droplet decreases, the total evaporation flux, J , tends to the value attained without Marangoni convection. To understand such

behaviour let us compare the two types of heat transfer in the system: conductive and convective.

In the first approximation, when convection is absent, the conductive heat flux from the substrate to the droplet surface is spent on evaporation (see Eq. (22)). If the heat flux to air is neglected, then we get from Eq. (22)

$$-k_l(\nabla T)_l \cdot \vec{n}_{l,a} = j \cdot \Lambda, \text{ that is } \frac{T_\infty - T_{apex}}{L} \sim j_{apex} \frac{\Lambda}{k_l}, \text{ where } T_{apex} \text{ is the temperature}$$

and j_{apex} is the local vapour flux at the droplet apex. According to (5) $j_{apex} \sim \frac{1}{L}$.

Comparing the latter two equations we conclude that $T_\infty - T_{apex}$ does not depend on the droplet size L . However, that latter is true only for the case of no MC (Fig. 11).

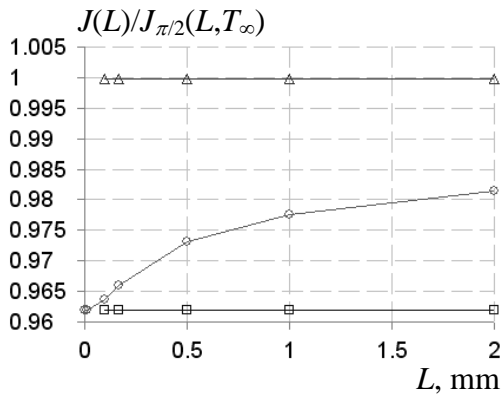


Fig. 10. Dependence of the total vapour flux from the droplet surface, J , on radius of the droplet base, L , at $\theta = \pi/2$. Circles - MC and LHV are taken into account; Squares - LHV is included, but MC is excluded; Triangles - both MC and LHV are excluded from the model.

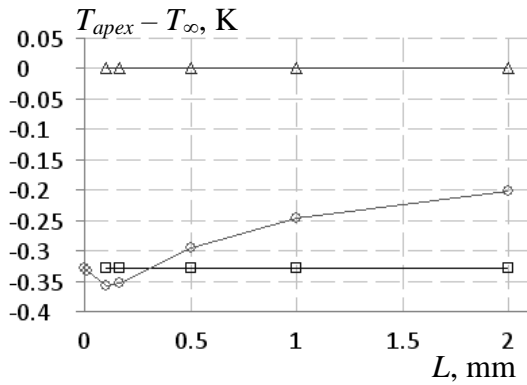


Fig. 11. Dependence of the temperature at the apex of the droplet, T_{apex} , on the radius of the droplet base, L , at $\theta = \pi/2$. Circles - MC and LHV are taken into account; squares - LHV is included, but MC is excluded; triangles - both MC and LHV are excluded.

According to the Newton's law of viscous flow, the velocity gradient in the droplet is proportional to the surface stress, Eq. (18):

$$\frac{u_{surf} - u_{sub}}{L} \sim |\gamma'_T| \frac{T_\infty - T_{apex}}{L}, \text{ where } u_{surf} \text{ is the velocity at the droplet surface,}$$

and $u_{sub} = 0$ is the velocity at the solid substrate. Consequently, $u_{surf} \sim T_\infty - T_{apex}$, which does not depend on the droplet size L .

Thus, in the first approximation the velocity inside the droplet is constant, leading to a constant convective heat flux. At the same time the conductive heat flux is proportional to the temperature gradient $\frac{T_\infty - T_{apex}}{L}$.

Therefore as the droplet size decreases the conductive regime of heat transfer becomes dominant. As a result (Fig. 10) the reduction of the droplet base radius, L , changes the value of total vapour flux, J , to that corresponding to the regime of heat conduction only.

Evaporation of a droplet placed on a heated substrate reveals similar dependencies of the total vapour flux, J , on the contact angle, θ , as shown in Fig. 12. In this case the total vapour flux, J , is related to the theoretical value,

$J_{\pi/2}$, according to Eq. (3), at a surface temperature equal to the temperature of the heated substrate. As before the result in the case of a copper substrate is close to the theoretical curve because of the high heat conductivity of copper and, consequently, the small difference in the temperatures of the droplet surface and the heated substrate. But for poorly heat conductive materials the deviation from the isothermal curve is even bigger than that in case of absence of substrate heating (Fig. 8).

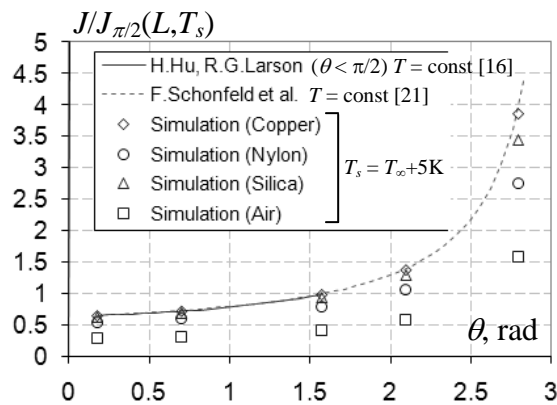


Fig. 12. Dependence of total vapour flux from the droplet surface, J , on contact angle, θ , in the case of substrate heating, $L = 1$ mm. Both LHV and MC are taken into account. Normalized by $J_{\pi/2}(L, T_s)$. T_s is the temperature of the substrate far from the droplet.

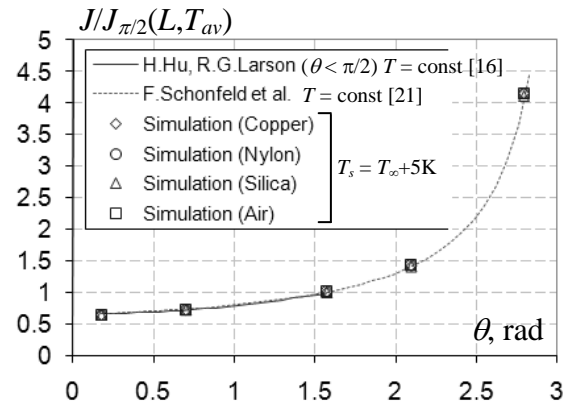


Fig. 13. Dependence of total vapour flux from the droplet surface, J , on contact angle, θ , in the case of substrate heating. $L = 1$ mm. Both LHV and MC are taken into account. Normalized by $J_{\pi/2}(L, T_{av})$. T_s is the temperature of the substrate far from the droplet.

Fig. 13 shows the same simulation results as shown in Fig. 12, but comparing with the theoretical value (Eq. (3)), $J_{\pi/2}$, calculated with the mean temperature of the droplet surface, T_{av} . It is clearly seen that all curves fall on one universal relationship. Thus, it can be concluded that the mean surface temperature of the droplet, T_{av} , is an important parameter to prescribe the evaporation rate together with droplet base radius, L , and contact angle, θ .

4. Conclusions

The evaporation of sessile droplets has been investigated in a self consistent way by considering an interconnected problem of vapour transfer, heat transfer in vapour, liquid and solid support, and Marangoni convection inside the liquid droplet. The influence of thermal conductivity of the solid support on the evaporation process has been analyzed. The calculated total evaporation flux is compared with the result in the case of isothermal evaporation. It has been shown that the lower the thermal conductivity of the solid support the higher the deviations appear from the isothermal case. However, if the mean temperature of the droplet surface is used instead of the temperature of the surrounding air for the vapour concentration on the droplet surface then the calculated dependences coincide with those calculated for the isothermal case.

It has also been found that the latent heat of vaporization does not change the qualitative dependence of the total vapour flux, J , on the droplet size, L . The dependence remains linear: $J \sim L$. The latent heat of vaporization affects only the distribution of the local flux over the droplet surface due to temperature changes and reduces the value of the total vapour

flux, J . This effect however does not change the proportionality of the local normal vapour flux at the apex of the droplet to the inverse value of droplet size: $j_{apex} \sim 1/L$.

The presence of the thermal Marangoni convection inside the droplet makes all the dependences non-linear. Consequently, the proportionality of the rate of change of the droplet volume to the radius of the droplet base, L , is affected by the thermal Marangoni convection inside the droplets.

If we plot the rescaled dimensionless total flux $J/J_{\pi/2}(L, T_{av})$, where T_{av} is the mean surface temperature, then all calculated total fluxes for substrates of different heat conductivity fall on one universal relationship between the total vapour flux, J , and the contact angle, θ . Accordingly, the variation of the surface temperature is the major element influencing the evaporation rate.

Acknowledgement

This research was supported by the European Union under Grant MULTIFLOW, FP7-ITN-2008-214919. V.M. Starov's research was also supported by the Engineering and Physical Sciences Research Council, UK (Grant [EP/D077869/1](#)). The work of R.G. Rubio was supported in part by the Spanish Ministerio de Ciencia e Innovación through grant FIS2006-12281-002-01, and by the Comunidad de Madrid through project INTERFASES (S-0505/MAT-0227).

References

- [1] M. Burger, R. Schmehl, K. Prommersberger, O. Schafer, R. Koch, S. Wittig, *Int. J. Heat Mass Transfer* 46 (2003) 4403–4412.
- [2] V. Dugas, J. Broutin, E. Souteyrand, *Langmuir* 21 (2005) 9130-9136.
- [3] Hyungmo Kim, Joonwon Kim, *J. Micromech. Microeng.* 20 (2010) 045008
- [4] S. Moosman, G.M. Homsy, *J. Colloid Interface Sci.* 73 (1980) 212–223.
- [5] F. Girard, M. Antoni, K. Sefiane, *Langmuir* 24 (2008) 9207–9210.
- [6] C. Bourges-Monnier, M.E.R. Shanahan, *Langmuir* 11 (1995) 2820–2829.

- [7] K. Sefiane, L. Tadrist, *Int. Commun. Heat Mass Transfer* 33 (2006) 482–490.
- [8] R.D. Deegan, *Phys. Rev. E* 61 (2000) 475–485.
- [9] R.D. Deegan, O. Bakajin, T.F. Dupont, G. Huber, S.R. Nagel, T.A. Witten, *Phys. Rev. E* 62 (2000) 756–765.
- [10] G. Guena, C. Poulard, M. Voue, J.D. Coninck, A.M. Cazabat, *Colloids Surfaces A* 291 (2006) 191–196.
- [11] R.G. Picknett, R. Bexon, *J. Colloid Interface Sci.* 61 (1977) 336–350.
- [12] F. Girard, M. Antoni, S. Faure, A. Steinchen, *Langmuir* 22 (2006) 11085–11091.
- [13] F. Girard, M. Antoni, S. Faure, A. Steinchen, *Microgr. Sci. Technol.* XVIII-3/4 (2006) 42–46.
- [14] F. Girard, M. Antoni, S. Faure, A. Steinchen, *Colloids Surfaces A* 323 (2008) 36–49.
- [15] F. Girard, M. Antoni, *Langmuir* 24 (2008) 11342–11345.
- [16] H. Hu, R.G. Larson, *J. Phys. Chem. B* 106 (2002) 1334–1344.
- [17] H. Hu, R.G. Larson, *Langmuir*, 21 (2005) 3963–3971.
- [18] H. Hu, R.G. Larson, *Langmuir*, 21 (2005) 3972–3980.
- [19] K.S. Lee, C.Y. Cheah, R.J. Copleston, V.M. Starov, K. Sefiane, *Colloids Surfaces A*, 323 (2008) 63–72.
- [20] K.P. Galvin, *Chem. Eng. Sci.* 60 (2005) 4659–4660.
- [21] F. Schonfeld, K.H. Graf, S. Hardt, H.J. Butt, *Int. J. Heat Mass Transfer* 51 (2008) 3696–3699.